JOURNAL OF SOLID STATE CHEMISTRY 3, 440–451 (1971

Examination of Substoichiometric WO_{3-x} Crystals by Electron Microscopy*

J. G. ALLPRESS

C.S.I.R.O.—Division of Tribophysics, University of Melbourne, Parkville, Victoria 3052, Australia

R. J. D. TILLEY

School of Materials Science, University of Bradford, Bradford, Yorkshire, U.K.

M. J. SIENKO†

Baker Laboratory of Chemistry, Cornell University, Ithaca, New York, 14850

Received February 3, 1971

The defect structure of high purity crystals of tungsten oxides with compositions between $WO_{3.00}$ and $WO_{2.99}$ has been investigated by transmission electron microscopy. The oxygen deficiency appears to be accommodated by Wadsley defects, disordered crystallographic shear planes, parallel to $\{120\}_R$ ($R = ReO_3$-type parent lattice). The planes tend to collect into bands which cause some regions of the crystal to have compositions far removed from the bulk. An observed maximum in carrier mobility is attributed to the destruction of conduction band states in the defect-rich regions. A modified form of the dislocation model for shear plane formation is proposed.

Introduction

In recent years a great deal of attention has been given to oxides containing, as the principal structural motif, crystallographic shear planes (*1*). This attention was initially centered on structures that contained regular and well-ordered crystallographic shear planes. These gave rise to X-ray diffraction patterns which, although difficult to interpret, could be solved by conventional techniques. The existence of the homologous series of oxide structures based upon the ReO_3 structure (*2, 3, 4*) and the rutile structure (*5*) established by these studies led to a great deal of speculation about the nature of defects in these materials. This centered largely upon the defect structure of the slightly reduced parent oxides, notably WO_{3-x}, TiO_{2-x}, and MoO_{3-x}. The two outstanding questions to be answered were (*a*) whether point defects or related defect clusters existed in these materials and (*b*) by what mechanism were crystallographic shear planes generated and caused to order in these oxides.

Oxygen deficiency in the transition metal oxides generally converts a broad-band intrinsic semiconductor to an extrinsic semiconductor having donor activation energy of about 0.01 eV. Under ambient conditions, each oxygen deficiency contributes roughly two carriers to the band. At low oxygen defect, it has been generally assumed that the missing oxygen atoms are removed randomly from the parent stoichiometric structure. However, recent studies on carrier characteristics in substoichiometric tungsten trioxide very close to stoichiometry (*6*) led to the inescapable conclusion that removal of oxygen is not random but segregated, even when x in WO_{3-x} is less than 0.0001. Given the increased confidence in conclusions drawn from several types of measurements (conductivity, Hall voltage, thermal emf, magnetic susceptibility, optical studies) made on the same crystals with well-defined chemical and thermal history, it was believed useful

* This research was supported in part by the Air Force Office of Scientific Research and the Advanced Research Projects Agency.

† On leave at the Laboratoire d'Electrostatique et de Physique du Metal, C.N.R.S.-Rayons X, Grenoble, France. The hospitality of Dr. E. F. Bertaut and the support of the John Simon Guggenheim Memorial Foundation are gratefully acknowledged.

to examine by electron microscopy the microstructure of crystals of WO_{3-x} for which the transport properties had been investigated.

Spyridelis, Delavignette, and Amelinckx (*7*) have examined crystals of WO_{3-x}, prepared from the vapor in flowing argon, and have observed arrays of regularly spaced dislocations lying perpendicular to the [001] direction of WO_3. They suggested that these were misfit dislocations lying between layers of slightly different composition. The departure from stoichiometry was undetermined.

Tilley (*8*) has prepared WO_{3-x} with $x \leqslant 0.02$ by reducing sublimed crystals of WO_3 in vacuo at temperatures up to 850°C. He showed that they contained planar defects parallel to $\{120\}_R$ (R = idealized cubic ReO_3 type lattice of WO_3) and concluded that these defects were crystallographic shear planes analogous to those found in the $(Mo, W)_nO_{3n-1}$ series of oxides (*4*).

Allpress and Gadó (*9*) have examined disordered samples with $x \approx 0.05$ and have observed crystallographic shear planes parallel to $\{130\}_R$. The structure of the ordered phase $W_{20}O_{58}$ (*2*) also contains regularly spaced crystallographic shear planes parallel to $\{130\}_R$. Using optical microscopy, Berak and Sienko (*6*) observed lines parallel to $\langle 120\rangle_R$ for small x; at higher x, lines parallel to $\langle 130\rangle_R$ began to appear.

Experimental Procedure

Materials

Ultra-pure WO_3 from Sylvania Electric Products was grown as stoichiometric crystals by the vapor-phase technique of Sawada and Danielson (*10*) and subsequently reduced by heating at 1022 ± 3°C for five days under various partial pressures of oxygen. The details of crystal growth and chemical analysis have been described elsewhere (*6*). The crystals described below ranged from $WO_{2.993}$ grown at $P_{O_2} = 5 \times 10^{-8}$ atm to $WO_{2.9999}$ grown at $P_{O_2} = 0.077$ atm. They were taken from the same batches as the crystals used for electrical transport measurements (*6*).

Technique

The samples were ground in an agate mortar, and small portions were collected on carbon-coated specimen grids for examination in a Philips EM200 or AEI EM6G electron microscope. Thin fragments were sought and were tilted until the electron beam was incident parallel to an axial direction. At this orientation, the fragments diffracted strongly. Images were recorded after tilting the fragment a few degrees about one of the axes perpendicular to the electron beam, in order to reduce the number of operating reflections and thereby increase the intensity of the transmitted beam (i.e., increase the transparency of the fragment). Most of the thin fragments had random shapes and areas of 1 to $5\mu^2$ (1 to 5×10^{-8} cm^2) perpendicular to the electron beam.

Electron diffraction patterns of all the samples were indexed in terms of an idealized ReO_3 type unit cell (cubic, $a \approx 3.8$ Å) rather than one of the slightly distorted cells of lower symmetry which apply to the various forms of WO_3, depending on the temperature (*11*). In general, it was not possible to establish the specific orientation with respect to a WO_3 cell with certainty because of the limited dimensional accuracy of the patterns and lack of knowledge of the temperature of the fragments during exposure to the electron beam. For this reason, we have chosen to identify the plane of each fragment which is perpendicular to (or nearly so) the incident electron beam as $(001)_R$.

Observations

(*a*) $WO_{2.994}$. A total of 50 different fragments of $WO_{2.994}$ were examined, part in the Philips EM200 and part in the AEI EM6G. They contained dark lines parallel to one or more of the $\langle 120\rangle_R$ directions, and the number and arrangement of these lines varied widely. When viewed with the electron beam exactly parallel to an axial direction, they were narrow and difficult to observe, but they became somewhat wider and very distinct after slight tilting (Fig. 1*a*). At larger tilts, fringe contrast typical of planar faults appeared (Fig. 1*b*, see also Fig. 5).

In most cases, the defects lay predominantly parallel to one of the $\{120\}_R$ planes, and they traversed the fragments from one side to the other (Fig. 2*a*). In these circumstances, the electron diffraction patterns displayed pronounced streaking of the Bragg reflections in the direction perpendicular to the plane of the defects (Fig. 2*b*). Occasionally, a defect was observed which terminated within a fragment, as at A in Figs. 1*a* and 2*a*, and many fragments contained a few defects lying on intersecting $\{120\}_R$ planes. In Fig. 1, they occur on all four of the $\{120\}_R$ planes which are parallel to the electron beam. Attempts were made to observe defects on the remaining $\{120\}_R$ planes which are inclined at angles of about 27° and 63° to the $(001)_R$ plane and intersect it in either the $[100]_R$ or $[010]_R$ directions. These attempts were unsuccessful, although a number of other planar faults which intersected $(001)_R$ near $[110]_R$ and $[1\bar{1}0]_R$ were observed (Fig. 3*a*).

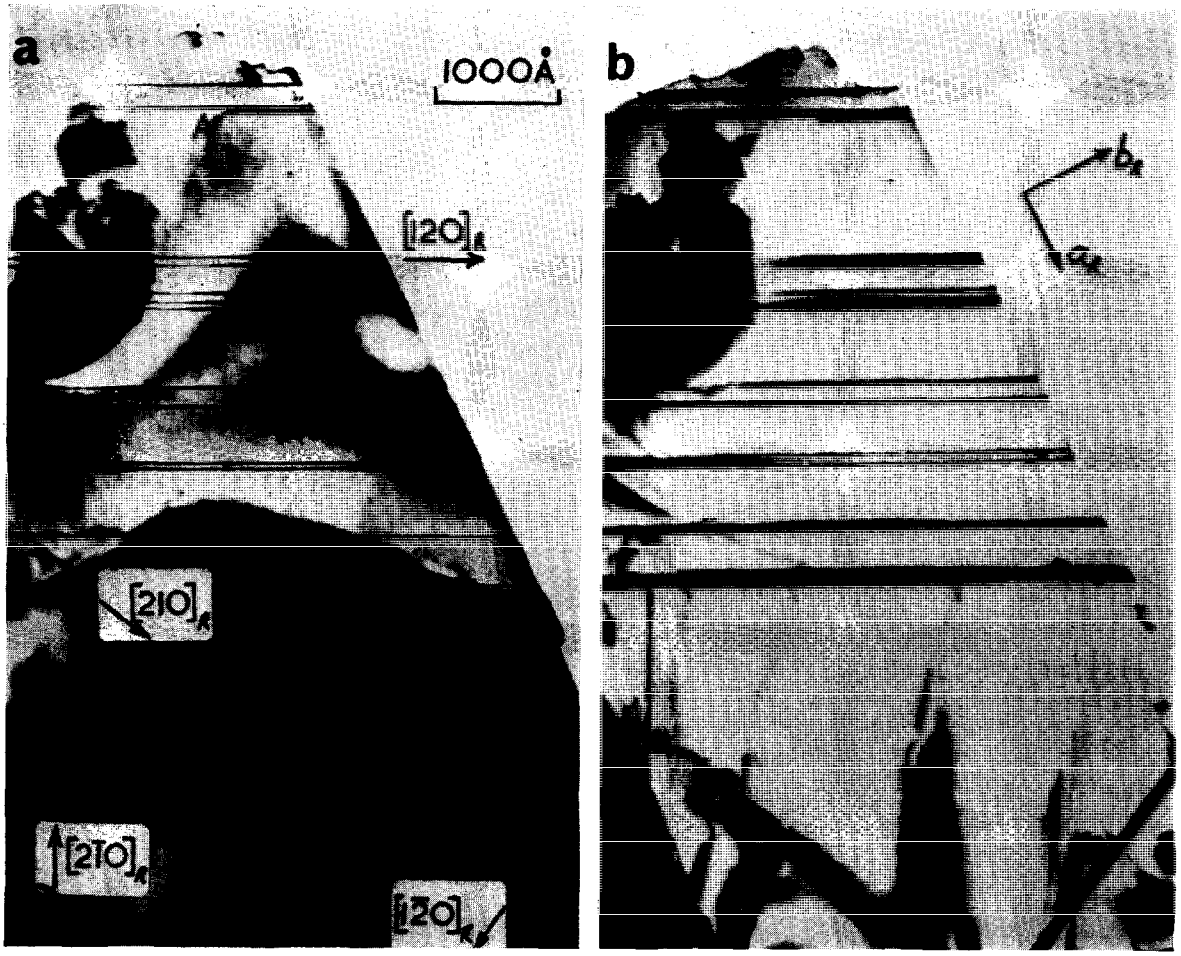

FIG. 1. (*a*) Planar defects parallel to $\{120\}_R$ in $WO_{2.994}$. The fragment is viewed almost parallel to an axial direction, and the defects appear as dark lines. Most of them lie along $[120]_R$, but a few are parallel to $[1\bar{2}0]_R$, $[210]_R$, and $[2\bar{1}0]_R$. At A one of the defects terminates within the fragment. (b) The same fragment after tilting a few degrees. All the defects, and particularly those parallel to $[120]_R$, show fringe contrast typical of planar faults.

The spacing between adjacent parallel faults varied from less than 100 Å to over 10,000 Å; groups of quasi-constant spacing were rarely observed. The mean spacing of 965 defects found in the 29 fragments examined in the Philips EM200 was 370 ± 270 Å. The very high standard deviation is a consequence of the wide variation in spacings and numbers of defects between fragments (cf. Figs. 1 and 2, for example).

(*b*) $WO_{2.9988}$. This sample was examined very briefly in the Philips EM200, and a total of 30 planar defects parallel to $\{120\}_R$ were observed in four fragments. It appeared that the defects tended to cluster in small groups, separated by large areas of unfaulted material. Some fragments did not contain any of these defects.

(*c*) $WO_{2.9999}$. This sample was examined in the Philips EM200. Planar defects parallel to $\{120\}_R$ were rarely observed in this sample. Other planar defects lying at an angle to $(001)_R$ and intersecting it near $[110]_R$ and $[1\bar{1}0]_R$ were more common. Figure 3*b* is an example, in which the $(120)_R$ defect appears as a narrow black line and the others as diffuse bands. Very large numbers of these inclined defects were often observed.

(*d*) $WO_{2.993}$. This sample was examined in the AEI EM6G. Again the most prominent defect structure was the presence of planar defects on $\{120\}_R$ planes. The concentration of defects was quite high and in some regions (Fig. 4) they were observed to be separated by the order of 40 Å. Diffraction patterns from these highly faulted

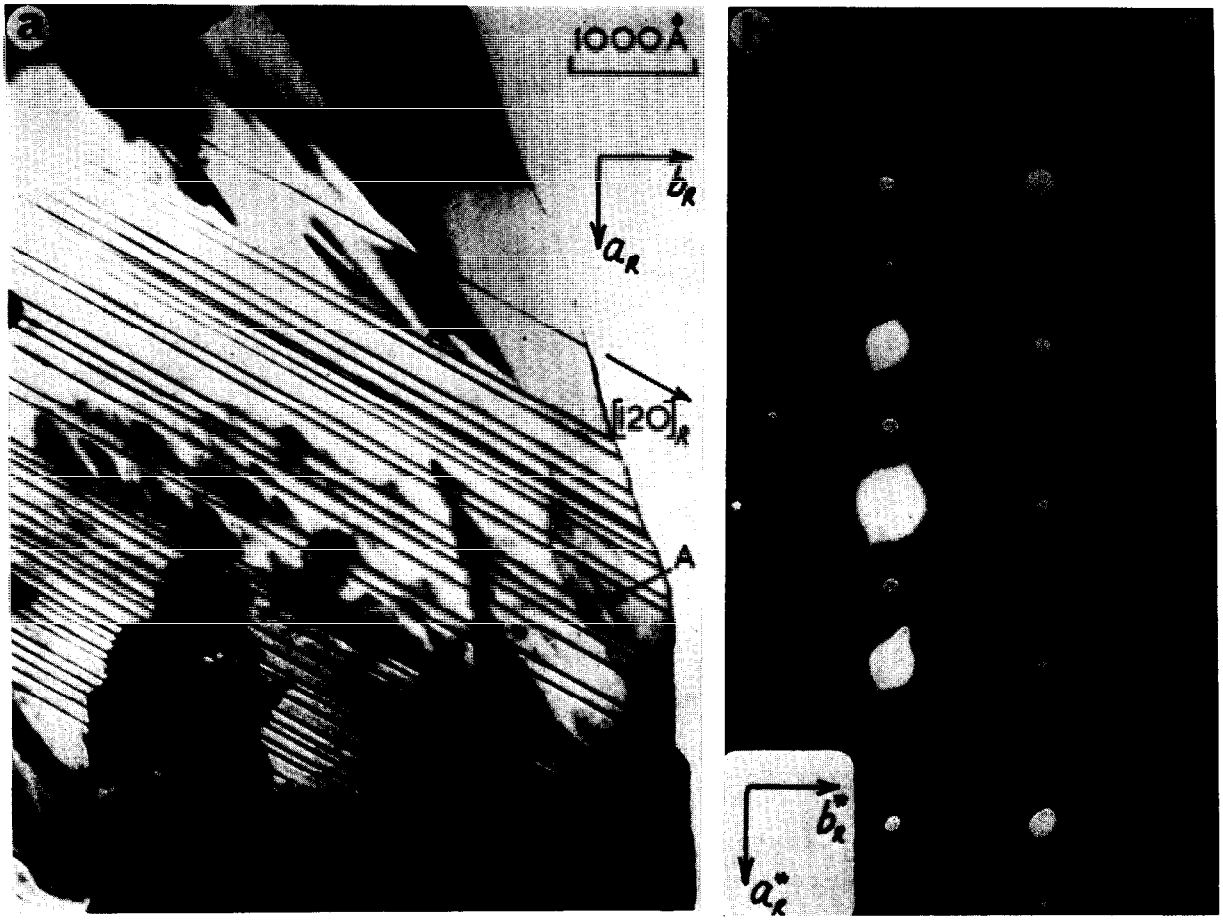

FIG. 2. (*a*) Planar defects parallel to $(120)_R$ in $WO_{2.994}$. In this fragment, the concentration of defects (black lines) is high, but their spacing is irregular. At A, one of them terminates within the fragment. (b) Electron diffraction pattern from the fragment shown in (*a*). The electron beam is incident a few degrees from $[001]_R$. The presence of the defects causes streaking of the Bragg reflections in the direction perpendicular to the plane of the defects.

regions showed a modulation in the streak intensity giving rise to apparent maxima and minima (Fig. 4*c*).

(*e*) $WO_{2.9993}$. This sample was examined in the AEI EM6G. Planar defects on $\{120\}_R$ planes were observed but far less frequently than in the sample (*d*). Isolated defects were not seen, and generally a flake contained either several defects or none at all. The inclined defects described in (*c*) above were observed in these crystals and, in fact, were seen far more often than the $\{120\}_R$ defects.

(*f*) $WO_{2.9963}$. This sample was briefly studied in the AEI EM6G. The defect structure was identical to that observed in the other samples described above.

(*g*) *Behavior of Defects During Electron Beam Heating.* Figure 5 shows two micrographs of $WO_{2.9999}$ which had been heated in the electron beam to an extent which caused the defects to grow and new ones to form. The fragment was projecting from the edge of a thick crystal, part of which can be seen at the top right of Fig. 5. Some of the heat generated by the absorption of the electron beam by the thick crystal was conducted into the fragment. Figure 5*a* was recorded after some defect growth had already occurred, although several of the defects were probably present prior to heating. The fault labelled P was observed to extend down through the fragment towards the cooler edge at the bottom of the figure. The rate of growth was of the order of 10^4 Å/sec. Figure 5*b* was taken after further heating by the focused electron beam for a few seconds and shows that a number of new defects have moved through the fragment, starting from the hottest part adjacent to the thick crystal. The orientation of the

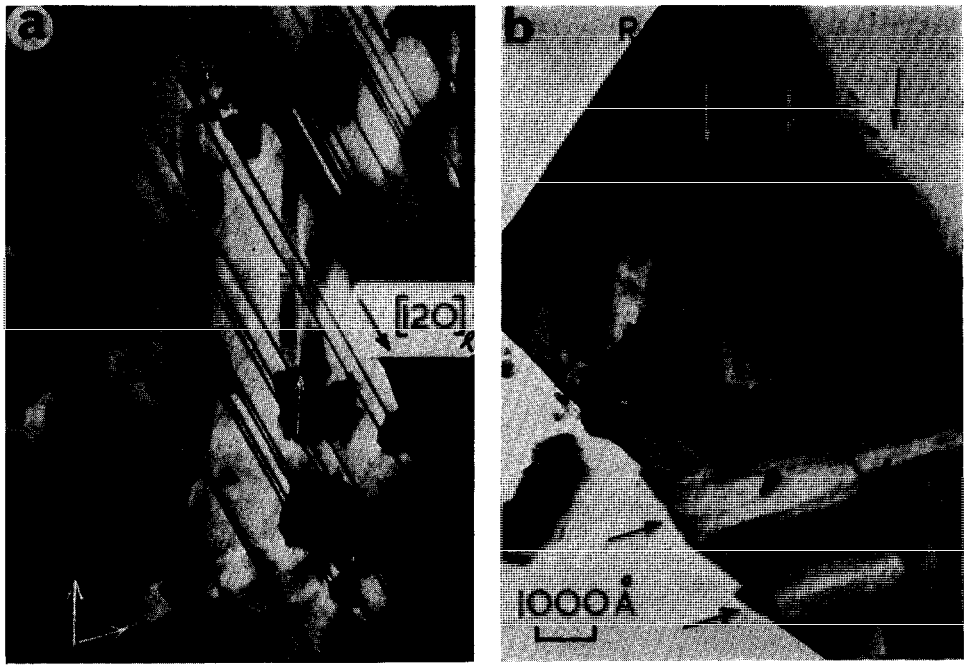

FIG. 3. (*a*) Micrograph of a fragment of $WO_{2.994}$, showing $(120)_R$ planar defects as straight black lines and additional inclined planar defects intersecting the surface near $[110]_R$ marked by white arrows. (*b*) Micrograph of a fragment of $WO_{2.9999}$ containing a single $(120)_R$ planar defect P and a number of inclined faults (arrowed) which are responsible for the variations in contrast over the fragment.

fragment is such that the defects, which all lie parallel to $\{120\}_R$ planes, are at an angle to the electron beam and, therefore, exhibit fringe contrast.

The inclined planar defects seen in Fig. 3 were very sensitive to heat treatment in the electron beam and could be induced to disappear completely by moderate exposure to the focused electron beam. Figure 6 shows a fragment which contained a relatively small number of these defects, oriented so they appear as sets of fringes. They always occurred in pairs and enclosed regions (e.g., T in Fig. 6) where the contrast differed from that of the matrix (M). The members of any pair lay at a small angle to each other and frequently intersected and terminated within a fragment, e.g., at I. Figure 6*b* was taken after several minutes of viewing the crystal under normal illumination conditions. The defects near A have disappeared completely while others have moved and altered the volume of the regions of dark contrast (T).

Discussion

(*a*) Influence of Defects on Stoichiometry

The planar defects parallel to $\{120\}_R$ observed here appear to be very similar to those observed by Tilley (*8*) and are almost certainly crystallographic shear planes. Their numbers decreased considerably as the stoichiometry of the samples approached $WO_{3.0000}$. In addition, the chance observation of their growth in a heated fragment (Fig. 5) is consistent with this interpretation, since it is known that oxygen is lost when WO_3 is heated in vacuo and that crystallographic shear planes are a likely means of accommodating this deficiency. It seems likely that the lines parallel to $\langle 120\rangle_R$ observed by Berak and Sienko in these samples with optical microscopy (*6*) were due to the presence of groups of crystallographic shear planes in this orientation. The optical results together with the electron microscope studies of Allpress and Gadó (*9*) suggest that further reduction can also be accommodated on $\{130\}_R$ planes.

The number of crystallographic shear planes in $WO_{2.994}$ is sufficiently large to enable an estimate to be made of their influence on the stoichiometry. In the absence of any other structural information we assume that the crystallographic shear planes parallel to $\{120\}_R$ in WO_{3-x} have the same structure as those in the series of phases $(Mo, W)_nO_{3n-1}$ (*12*). It is a straightforward matter, then, to show that the spacings of shear planes in an ordered structure of

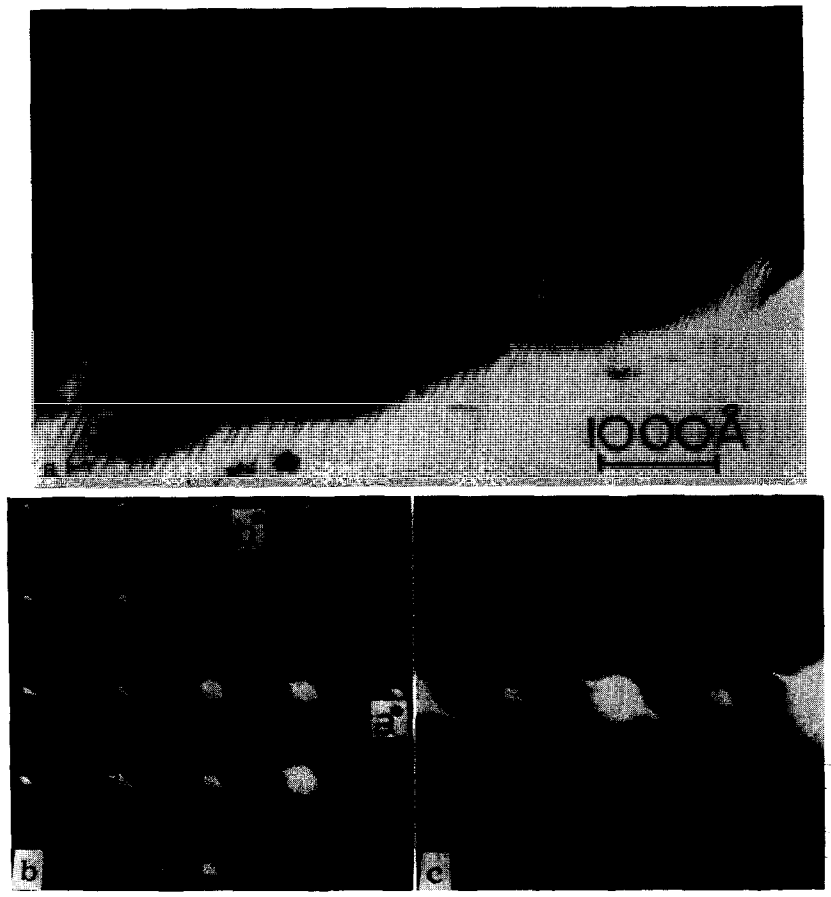

FIG. 4. (*a*) Defects on $(\bar{2}10)$ planes in $WO_{2.993}$. The region A contains quasi-ordered faults with a spacing of 40–50 Å. A mistake in the fault sequence is also present in this region. (*b*) Diffraction pattern from the region shown in (*a*) after the crystal has been tilted a few degrees. (*c*) Enlargement of part of the streaking through the diffraction spots, showing a modulation of the streak with a periodicity of approximately 42 Å.

composition M_nO_{3n-1} is given by

$$S = \frac{2n-1}{2}\frac{a}{\sqrt{5}}$$

where a is the lattice parameter of the idealized cubic structure of WO_3. Since $a \approx 3.8$ Å, we obtain $S = 0.85\,(2n-1)$ Å. If our sample of $WO_{2.994}$ were completely ordered with all its nonstoichiometry accommodated in a single set of crystallographic shear planes parallel to one of the $\{120\}_R$ planes, we would have $WO_{2.994} = W_{167}O_{500}$—i.e., $n = 167$ and $S = 283$ Å. This spacing is of the correct order of magnitude, since the observed mean spacing was 370 ± 270 Å. A similar calculation gives a spacing of 17000 Å for hypothetical ordered $WO_{2.9999}$. This is consistent with the observation that shear planes in crystals of this composition were rarely observed. The fact that they were observed at all suggests that the intrinsic concentration of point defect oxygen vacancies is very small and contributes insignificantly to the total nonstoichiometry of WO_{3-x} for $x > 0.0001$.

Our observations included those of planar defects which intersected $(001)_R$ near $[110]_R$ and $[1\bar{1}0]_R$ (Figs. 3 and 6). The appearance of these defects in Fig. 6 indicates that they are domain boundaries, separating wedge-shaped regions (T) differing in orientation from that of the matrix (M). Their tendency to disappear during beam heating (Fig. 6) clearly distinguishes them from the crystallographic shear planes, which were observed to extend and increase in number under these conditions (Fig. 5). Similar domains have been observed by optical microscopy (*6*, *13*) in crystals of WO_3 which have been subjected to external stresses. Hence we believe that they are produced during the grinding processes

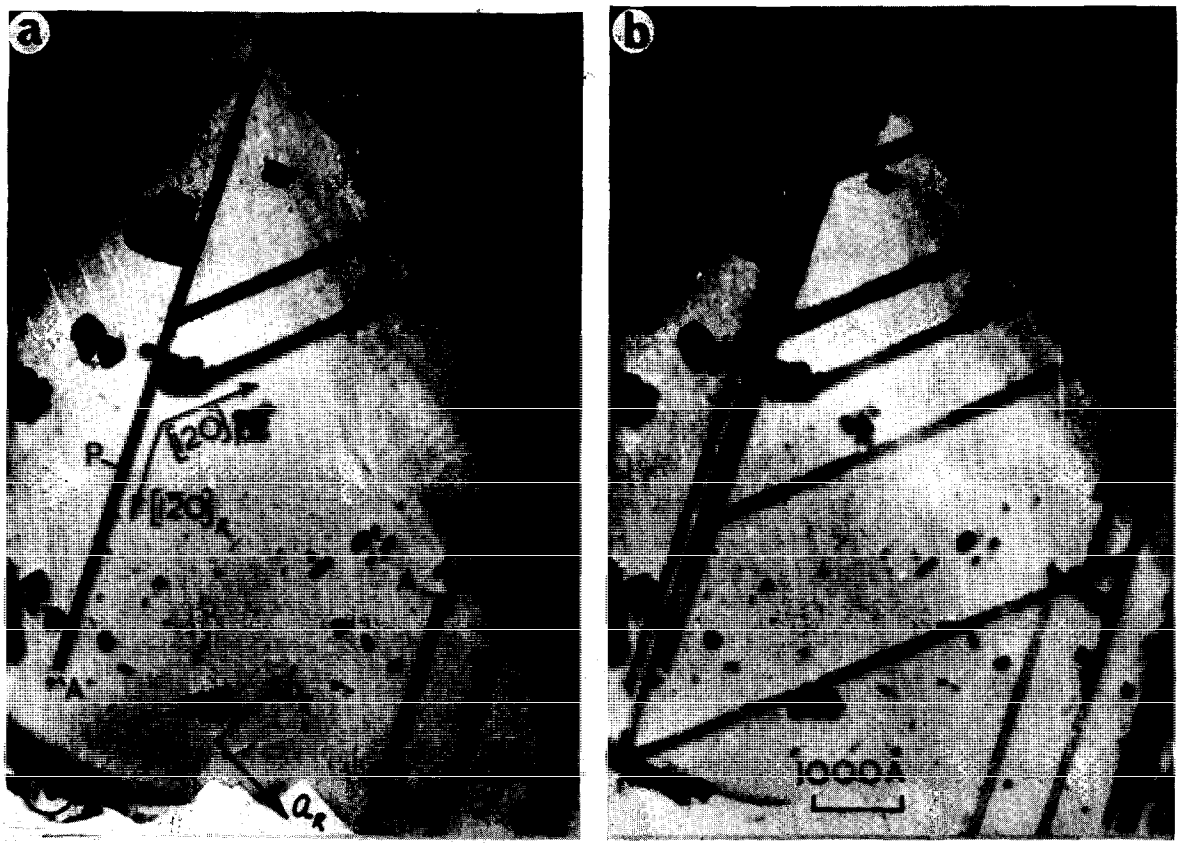

FIG. 5. Planar $\{120\}_R$ defects in a fragment of $WO_{2.9999}$. This thin area was projecting from a thick crystal (at the top right of the figure) which acted as a source of heat during electron beam illumination. (*a*) was recorded after some defect growth had occurred; the fault labelled P was observed to extend down through the fragment from the hotter area near the thick crystal. (*b*) was recorded shortly after and shows the formation of a number of additional defects of the same kind.

involved in the preparation of thin fragments for electron microscopy and are *not* associated in any way with departures from stoichiometry. It seems probable that the domains are mechanical twins in the monoclinic phase, which are removed entirely when the material is heated beyond the monoclinic-tetragonal temperature of 750°C (*11*).

(*b*) Mechanism of Formation and Growth of Shear Planes

The mechanism by which crystallographic shear planes are formed has been treated theoretically from three standpoints. First, Gadó (*14*), using evidence from X-ray diffraction studies, invoked large point-defect concentrations which formed walls through the crystal at the point where crystallographic shear planes were eventually to form. Eventual collapse of the crystal at these walls eliminated the vacancies and formed the crystallographic shear planes. Anderson and Hyde (*15*) proposed a dislocation model which also as a prerequisite needed a point-defect concentration in the lattice over and above the intrinsic defects expected. In both of these models, therefore, the initial step of reduction was the introduction of point defects or related species. Andersson and Wadsley (*16*), using structural evidence, considered that such a concentration of point defects was unlikely and derived a mechanism for the formation of crystallographic shear planes which did not involve any point defects at all and which, at the same time, could account for their ordering.

Gadó's proposal should lead one to observe ordered vacancies in the slightly reduced material. Electron diffraction is particularly sensitive to such microstructure due to the high degree of interaction between electrons and the crystal lattice. Although intense streaking was observed in diffraction

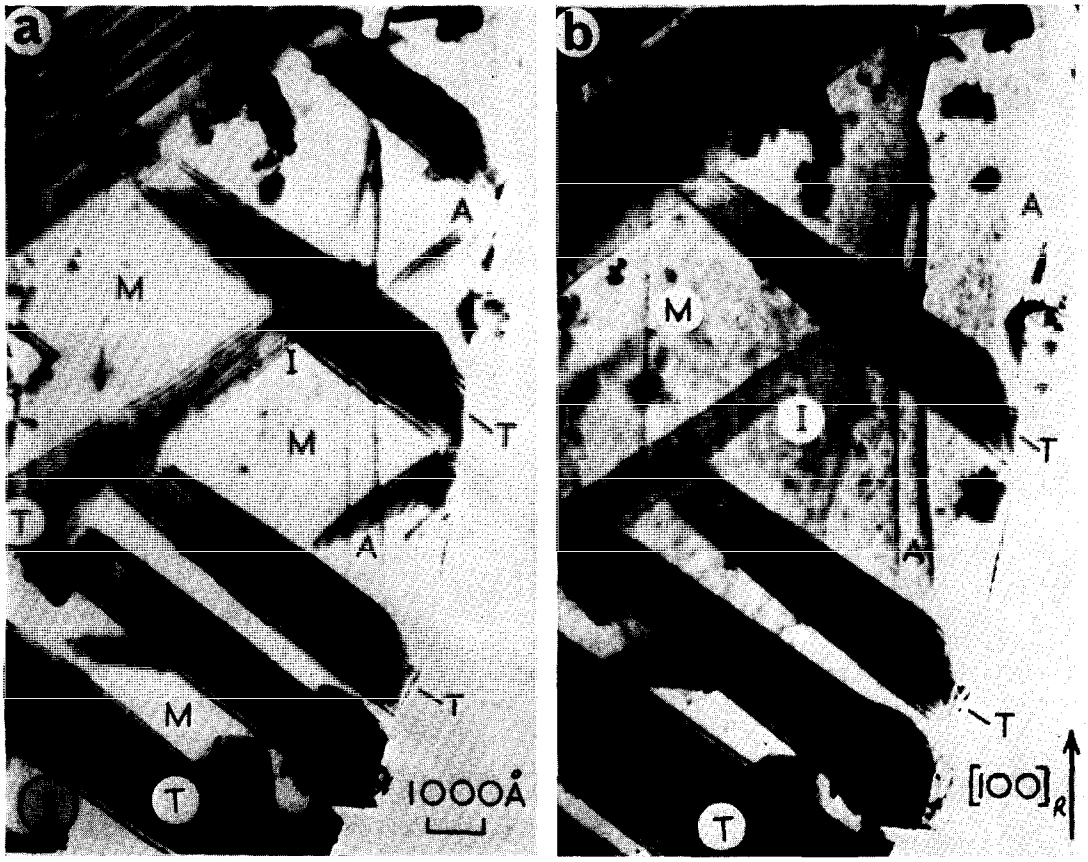

FIG. 6. (*a*) Inclined planar defects in $WO_{2.9999}$. These defects occur in pairs bounding wedge-shaped regions T in the matrix M. (*b*) After a short period of observation the defects near A in (*a*) have disappeared completely, and others have migrated. The volumes of the regions T have altered, and the end of the wedge at I has moved.

patterns, no traces of superlattice reflections were seen; this suggests that vacancy ordering is not taking place.

Vacancies are an essential part of the Anderson and Hyde model, and in this case they could well exist as either ordered or disordered entities. The argument against an ordered array is again valid, but it is far harder to investigate the existence of disordered point defects. The lack of any diffuse scattering on diffraction patterns of these crystals is, however, an indication that such disorder, if it exists, is relatively low. The basis of this model is the aggregation of vacancies into discs, which eventually expand to form shear planes. Hence, at some degree of substoichiometry one would expect to observe these loops and small segments of shear planes intermediate in size between the loops and a fully developed structure. Such partial defect structures have not been observed in any crystals studied, the defect structures always consisting of well-developed shear planes of appreciable length.

The model of Andersson and Wadsley involves creation of complete shear planes at the surface, followed by lateral migration into the crystal. At small degrees of nonstoichiometry one would, therefore, expect a distinct segregation between the bulk of the crystal and the exterior regions. From the point of view of electron microscopy, such segregation is hard to disprove, as only small regions of materials are examined, and it is difficult to be categorical about the position of the flake in the original crystal. However, two other observations are in conflict with the Andersson–Wadsley model: (1) Some shear planes (A in Figs. 1 and 2) terminate within the crystal. (2) Shear planes in Fig. 5 were seen to extend along their lengths but not move laterally. Lateral migration might well be involved in the ordering of planes but apparently not in their formation and growth. Optical microscopy suggests that the defects form as planes situated at random, whereas the model of Andersson and Wadsley suggests ordered growth from one or two regions of

the crystal. As discussed in more detail below, the development of crystallographic shear planes shown in Fig. 5 is not in agreement with the Andersson–Wadsley model at all but does agree with that of Anderson and Hyde.

The observed clustering of shear planes in WO_{3-x} together with the precise ordering observed in the ordered oxides based on shear suggest that the ordered state is energetically favorable. The presence of disordered defects and the evidence of Fig. 5 makes the dislocation model of Anderson and Hyde most in accord with the experimental results. However, the absence of dislocation loops or of diffuse scattering on diffraction patterns suggests that the collapse of discs of vacancies does not take place. If the crystallographic shear planes are considered to nucleate at the surface, the need to introduce point defects into the crystal lattice becomes redundant. Strain at the dislocation centered on the end of the shear plane in the body of the crystal could then cause it to act as a site of enhanced chemical reactivity. Thus, further oxygen loss is likely to take place along this line causing a growth of the defect into the matrix of the crystal in an analogous fashion to that suggested by Anderson and Hyde. The oxygen atoms so released would in all probability migrate along the dislocation line to the surface, but as most oxides which form shear structures have high oxygen diffusion coefficients, this need not be essential.

A diagram of the termination of a $(\bar{2}10)$ shear plane is shown in Fig. 7. The WO_3 structure has been idealized for simplicity, and the actual structure of the dislocation core is hypothetical. The process of losing a surface oxygen and the subsequent rearrangement of the lattice is shown diagrammatically in Fig. 8. It is envisaged that the process is repeated at other depths within the crystal, with the redundant oxygen ions migrating to the surface. The process by which the octahedra rearrange to form blocks is schematic. The diffusion of tungsten atoms will be by way of triangular faces of the surrounding octahedra of anions, this being the easiest path geometrically. Which face is selected will depend on lattice distortions in the neighborhood of the dislocation bounding the planar fault, which will be different from the distortions met with in the bulk.

The amount of oxygen lost during the rearrangement process will be reflected in the number of octahedra which share edges. The simplest way this can happen is for two octahedra to link an edge (Fig. 9). In this case, however, no oxygen is lost. Mechanistically, this is equivalent to having the displacement vector of the fault lie in the fault plane.

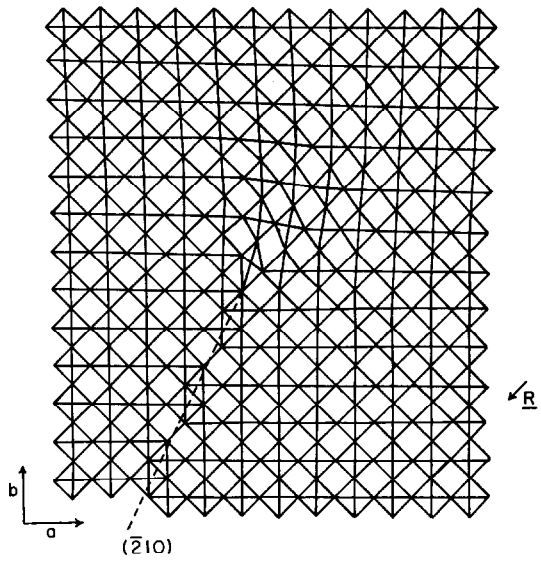

FIG. 7. Diagrammatic representation of the termination of a $(\bar{2}10)$ crystallographic shear plane in the idealized WO_3 structure. The vector R is the shear vector of the fault.

The next most simple mode of linking is that shown in Figs. 7 and 8. For every two octahedra linked to the initial pair, one oxygen atom is lost, and a linkage of four octahedra provides the smallest degree of reduction possible along a plane. Repeating this mechanism forces the shear plane to line along $\{120\}_R$ planes, and hence it is clear that the lowest degree of reduction in these crystals will be accommodated along $\{120\}_R$ planes.

The next stage in reduction is to link six octahedra. This is done in an analogous fashion to linking four,

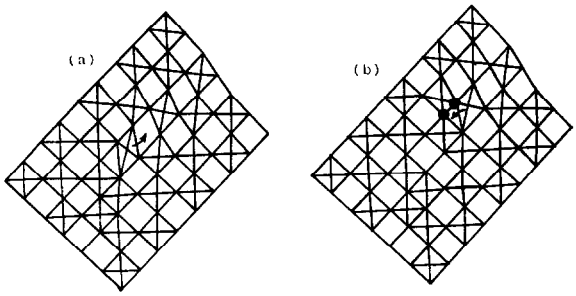

FIG. 8. (*a*) Initial step in the linkage of four octahedra in the idealized WO_3 structure is shown by the arrow. This leads to the situation shown in (*b*). No oxygen is lost at this step. (*b*) Second step in the linkage, shown by the arrow. One of the pair of oxygens shown as ● is lost at this step. After this step the crystal has the appearance shown in Fig. 7 and 8*a*. The orientations of Figs. 7 and 8 are identical, and they can be superimposed in order to reveal the rearrangement more clearly.

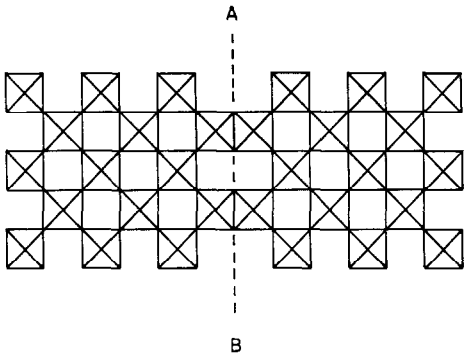

FIG. 9. The simplest shearing process in the idealized WO_3 lattice. The boundary AB is on (110) and does not involve oxygen loss. It can be regarded as an antiphase boundary or twin boundary.

the final step only being continued to another pair (Fig. 10). As can be seen, repeating this process leads to $\{130\}_R$ Wadsley defects. This process causes two oxygen atoms to be lost in the linkage of six octahedra.

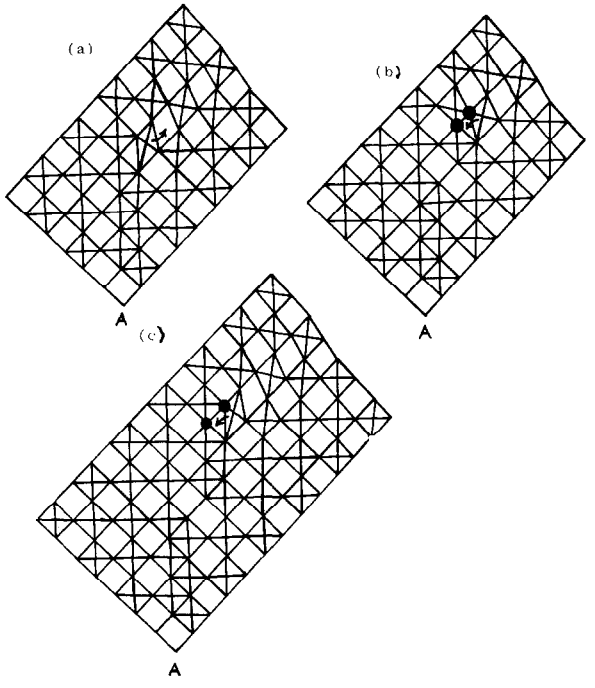

FIG. 10. (*a*) Initial step in the linkage of six octahedra in the idealized WO_3 structure is shown by the arrow. This leads to the situation shown in (*b*). No oxygen is lost at this step. (*b*) Second step in the linkage. One of the pair of oxygens shown as ● is lost, and the situation shown in (*c*) exists. (*c*) Final step in the linkage. Another one of the pair of oxygens, ●, is lost and after this step the situation shown in (*a*) again prevails. *A* refers to the origin of the diagram, and (*a*) and (*c*) can be superimposed at *A* to show the dislocation movement.

It is possible to continue such linkages indefinitely. Linking eight octahedra loses three oxygen atoms and leads to $\{140\}_R$ defects. Linking ten octahedra loses four oxygen atoms and leads to $\{150\}_R$ defects. The ultimate step is the linkage of strings of octahedra, such as occurs in the idealized V_2O_5 structure.

Whether the initial defects in real crystals of WO_{3-x} form preferentially on $\{210\}_R$ or $\{120\}_R$ depends on the distortions of the WO_6 octahedra present in the real structure. Projections of this structure, calculated from the data of Loopstra and Boldrini (*17*) and shown in Fig. 11, reveal that these distortions are considerable. This also shows that not all $\{120\}_R$ type planes are parallel to planes of tungsten atoms, so that the geometrical construction described by Anderson and Hyde is possible for a more limited number of planes.

At this point again it is worth considering the information contained in Fig. 5 which shows the dynamic growth of crystallographic shear planes. The preceding discussion of their formation attempted to correlate the final defect structure of crystals as

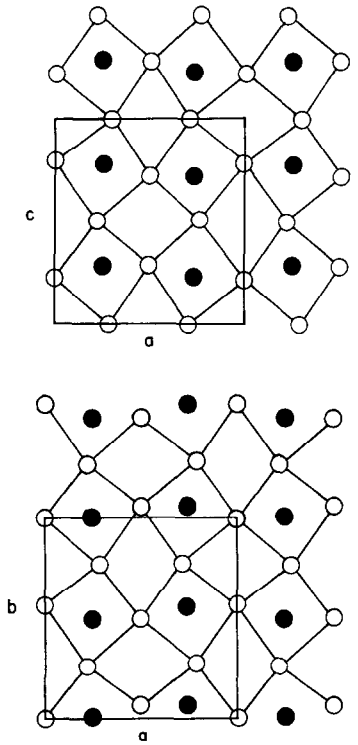

FIG. 11. (*a*) Section through the WO_3 structure at $y = 0$. (*b*) Section through the WO_3 structure at $z = 1/4$. In (*a*) and (*b*) the oxygen atoms (open circles) are linked by lines, and both the oxygen and tungsten atoms (filled circles) are staggered slightly above or below the plane of the paper.

the degree of substoichiometry decreased with the probable initial formation of the planar faults. There is clearly some danger in extrapolating the dynamic growth observed under the conditions in the electron microscope with expected growth under the preparative conditions used. In particular, the main differences are the bombardment of the now very thin sample in the electron microscope with (chemically reactive) electrons and the rate of growth: several minutes in the electron microscope compared with several days during original sample preparation. With this in mind, it is possible to say that the sequence of events shown in Fig. 5 is in agreement with the original Anderson and Hyde model. Perhaps more important is the fact that shear plane growth observed is in disagreement with the models of both Gadó and Andersson–Wadsley and provides evidence for the acceptance of a dislocation model in the dynamical situation, if not in all cases.

(*c*) Effect of Shear Planes on Electrical Transport Properties

As to influencing the electrical transport properties, the introduction of crystallographic shear planes has two effects: (1) to increase the carrier density, and (2) to decrease the carrier mobility. In stoichiometric WO_3, Crowder and Sienko (*18*) have shown that the conductivity arises through excitation of electrons from shallow donor impurity levels to the normally empty conduction band of tungsten trioxide in which the excited carriers move with polar scattering by longitudinal optical-mode lattice vibrations. In nonstoichiometric WO_{3-x} each missing oxygen atom contributes two electrons to the potential pool of carriers. At very low oxygen defect, i.e., $WO_{2.9999}$, all these carriers appear to be free, since the observed number of carriers was found to be (*6*) approximately equal to that calculated from the sum of the impurities and the oxygen defect. At higher oxygen defect, the observed number of carriers was approximately one fourth of that predicted, suggesting that there is trapping of carriers, probably at the crystallographic shear planes. More significantly, it was observed that as the oxygen defect increased there was a change in the character of the temperature dependence of mobility from polar mode lattice scattering to hopping. Berak and Sienko suggested (*6*), and the present studies bear this out, that the nonstoichiometric WO_{3-x} consists of two regions, defect and defect-free, in which the conduction processes differ. In the defect-free region, i.e., stoichiometric WO_3, conduction is by band processes, probably involving the W(5d)—O$p\pi$—W(5d) antibonding band (*19*). In the defect region, band processes probably do not occur. As shown by Mott (*20*) and Mott and Allgaier (*21*) fluctuations in composition can replace band states with localized states above the bottom of the conduction band. If the disorder is large, there may result destruction of band states in the physically accessible range of energies available to the electrons. In such a case, the excess electrons resulting from oxygen deficiency would occupy these localized states, and conduction in the defect region could take place only by way of phonon-activated hopping processes between levels. The hopping mode in the defect region would then exist in series with band behavior in the defect-free region.

The crystallographic shear planes are characterized by W—W overlap distances considerably smaller than those in the normal WO_3 matrix—viz., 3.8 Å instead of 5.3 Å. Even these W–W distances are probably not small enough for large overlap of the W5dt_{2g} orbitals, but the incipient W—W bonds could act as traps to break up the band processes existing elsewhere in the structure. The traps cannot be too deep, otherwise the observed density of carriers would be less than that calculated from impurity donors alone. Shallow traps, on the other hand, from which thermal energy would suffice to redissociate carriers, would be precisely what would be required to give a decreased carrier mobility as is observed.

Acknowledgment

This paper is the outcome of a collaborative effort between widely separated laboratories, the major contributions of each author being as follows: J. G. Allpress—observations on (*a*), (*b*), (*c*) and (*g*) with Philips EM 200 microscope, correlation of numbers of shear planes with stoichiometry; R. J. D. Tilley—observations on (*a*), (*d*), (*e*), (*f*) with AEI EM6G microscope, mechanism of formation and growth of shear planes; M. J. Sienko—supply of samples, coordination of data, correlation of results with electrical transport properties. We are indebted to J. M. Berak for growing the original crystals and to Dr. J. V. Sanders for helpful discussions and criticism.

References

1. A. D. Wadsley, *Rev. Pure Appl. Chem.* **5**, 165 (1955).
2. A. Magnéli, *Arkiv Kemi* **1**, 513 (1950).
3. P. Gadó and A. Magnéli, *Acta Chem. Scand.* **19**, 1514 (1965).
4. B. Blomberg, L. Kihlborg, and A. Magnéli, *Arkiv Kemi* **6**, 133 (1953).
5. S. Andersson and L. Jahnberg, *Arkiv Kemi* **21**, 413 (1963).

6. J. M. BERAK AND M. J. SIENKO, *J. Solid State Chem.* **2**, 109 (1970).
7. J. SPYRIDELIS, P. DELAVIGNETTE, AND S. AMELINCKX, *Mat. Res. Bull.* **2**, 615 (1967).
8. R. J. D. TILLEY, *Mater. Res. Bull.* **5**, 813 (1970).
9. J. G. ALLPRESS AND P. GADÓ, *Crystal Lattice Defects* **1**, 331 (1970).
10. S. SAWADA AND G. C. DANIELSON, *Phys. Rev.* **113**, 803, 1005 (1959).
11. R. S. ROTH AND J. L. WARING, *J. Res. NBS A* **70**, 281 (1966).
12. A. MAGNÉLI, *Acta Cryst.* **6**, 495 (1953).
13. S. TANISAKI, *J. Phys. Soc. Jap.* **13**, 363 (1958).
14. P. GADÓ, *Acta Phys. Hung.* **18**, 111 (1965).
15. J. S. ANDERSON AND B. G. HYDE, *J. Phys. Chem. Solids* **28**, 1393 (1967).
16. S. ANDERSSON AND A. D. WADSLEY, *Nature* **211**, 581 (1966).
17. B. O. LOOPSTRA AND P. BOLDRINI, *Acta Cryst. B* **25**, 1420 (1969).
18. B. L. CROWDER AND M. J. SIENKO, *J. Chem. Phys.* **38**, 1576 (1963).
19. J. C. GULICK AND M. J. SIENKO, *J. Solid State Chem.* **1**, 195 (1970).
20. N. F. MOTT, *Advan. Phys.* **16**, 49 (1967).
21. N. F. MOTT AND R. S. ALLGAIER, *Phys. Status. Solidi* **21**, 343 (1967).